ELSEVIER

Biophysical Chemistry 56 (1995) 241–261

Biophysical Chemistry

Photoacoustic diagnostics of fast photochemical and photobiological processes. Analysis of inverse problem solution

Oleg V. Puchenkov *,[1]

The Weizmann Institute of Science, Biochemistry Department, 76100, Rehovot, Israel

Received 24 November 1994; revised 8 February 1995; accepted 10 February 1995

Abstract

Photoacoustic (PA) diagnostics is a time-resolved experimental technique that measures transient photoinduced volume changes on the nano- and microsecond time-scales. The technique has been used to study the energetics and dynamics of chemical and biochemical reactions initiated by absorption of light. The dynamics of the volume changes and associated relaxation processes can be restored from PA-waveforms by solving an ill-posed problem of deconvolution. For the systems with known relaxation kinetics scheme this problem is usually solved by an iterative approximation algorithm. In complex photoactive systems (e.g. photosynthetic samples), where information about kinetics of fast photoinduced volume changes is not available, an algorithm of direct deconvolution must be used. The implementation of one of the linear deconvolution algorithms (Tikhonov's α-regularization) for the PA-diagnostics is therefore considered. The problem of the optimal choice of experimental set-up, and restoration algorithm is analyzed by a numerical simulation. It is shown that the quality of PA-diagnostic experiment is mainly determined by a transfer function converting the relaxation spectrum to the spectrum of output electric signal. The analytical expressions to calculate this function (so called PA-filter) are presented. The performance of two widely used schemes of PA-diagnostics are then directly compared. The time-resolution of the PA-diagnostics in analysis of simultaneous bi-exponential decay is evaluated, and the relationship between the resolving power and parameters of the experimental set-up (signal-to-noise ratio, sampling rate, shape of the PA-filter) is found. The advantage of front face irradiation scheme with piezopolymer film detector for time-resolved measurements is demonstrated.

Keywords: Photoacoustic diagnostics; Photoinduced volume changes; Relaxation kinetics; Inverse problem; Regularization algorithm; Numerical simulation

1. Introduction

Direct measurements of acoustic transients following the absorption of a laser pulse in a sample provide valuable kinetic information on the excited states in photoactive biological and chemical systems [1]. This photoacoustic (PA) method is especially useful for discrimination between channels of deactivation associated with luminescence and heat release. Analysis of photoacoustic waveforms may be used also to examine photoinduced phase transitions and chemical reactions [2,3]. Recently, time-resolved

* Corresponding author.

[1] Permanent address: N.N. Andreev Acoustics Institute, 117036, Moscow, Russia.

0301-4622/95/$09.50
SSDI 0301-4622(95)00036-4

PA-technique has been applied to the study of photoinduced transient volume changes in complex biological structures, for example, in bacteriorodopsin [4], and photosynthetic bacterial reaction centers [5]. In these species in addition to volume changes associated with the thermal expansion there exists non-thermal contribution to the PA-signal, e.g. conformational changes in proteins [6]. Therefore, accurate analysis and interpretation of PA-data can give valuable information about fast dynamics of structural reorganization in complex photoactive biological systems.

The method that one should apply to restore the dynamics of photoinduced volume changes depends substantially upon existence of an a-priori information about the nature of the underlying process. Usually, a kinetic model for the process of interest must be assumed which relies upon prior kinetic and quantum yield studies [3]. In the simplest case of pure exponential relaxation there is an explicit information about functional dependence of the volume changes upon time. Therefore, iterative approximation techniques based on nonlinear least squares fitting of experimental data by the sum of exponentials may be applied. The minimal time constant of the exponential decay resolved by the deconvolution technique was reported to be comparable with the digitization channel width [7]. However, the approximation algorithms cannot be directly used to restore the dynamics of complex relaxation processes when prior information on the kinetics is not available [4,5]. In this case the time dependence (or the equivalent frequency spectrum) of the photoinduced volume changes should be found by a direct deconvolution, then some reasonable mechanism of the relaxation can be suggested, and parameters of the theoretical kinetic scheme can be estimated. One possible way to construct the numeric algorithm for direct deconvolution will be discussed here.

Practical implementation of the PA-diagnostics needs the proper choice of the experimental set-up, which is characterized by the potential time resolution, achievable signal-to-noise ratio (S/N), and robustness to experimental errors. In the present analysis two different experimental set-ups are directly compared, and their use for relaxation kinetics measurements is evaluated.

2. Photoacoustic diagnostics as inverse problem

General experimental layout of the PA-measurements may be outlined as follows. An incident laser beam of intensity $i(t)$ (with a corresponding Fourier spectrum $I(\omega)$) is absorbed in a medium to produce molecules in an excited state which relax to the ground state according to some scheme of deactivation. The deactivation is accompanied by local volume changes in the region of light absorption due to heat release, and photoinduced rearrangement of the molecular structure of the sample. We shall consider the case when the laser-induced relative volume change $\nu(t)$ is proportional to the energy of laser pulse and can be expressed through the light intensity $i(t)$ in the form of convolution integral:

$$\partial\nu(t)/\partial t = \int_{-\infty}^{+\infty} r(t-\tau)i(\tau)\mathrm{d}\tau \qquad (1)$$

where $r(t)$ is the function of relaxation kinetics. Eq. (1) has a simple form in the frequency domain:

$$V(\omega) = R(\omega)I(\omega)$$

where $R(\omega)$, $I(\omega)$, and $V(\omega)$ are Fourier transforms of the functions $r(t)$, $i(t)$ and $\partial\nu/\partial t$, respectively. In the present analysis we shall assume that all the characteristic times of the problem are much smaller than the time of thermal diffusion, so the process of thermal diffusion on the time scale of experiment may be neglected. In this approximation the absolute magnitude of the function $\nu(t)$ may not decrease with time, and it is more convenient to consider its derivative for which correspondent Fourier spectrum may be introduced. The function $r(t)$ introduced by Eq. (1) is a more general than the ordinary relaxation function used in photochemical kinetics. The precise meaning of this function depends upon the nature of the underlying process of photoinduced volume changes (e.g., thermal expansion, electrostriction, or structural rearrangements in biological species [4,5,8]). For example, for a system where volume changes are produced only by the thermal expansion, and the heat release is determined by a single exponential decay of an excited state with a lifetime τ_a, one can write for $r(t)$:

$$r(t) = \frac{\mu\beta}{\rho C_p}\frac{\phi}{\tau_a}\exp\left(-\frac{t}{\tau_a}\right)$$

where μ is the optical absorption coefficient, ρ is the density of the medium, β and C_p are the thermal expansion coefficient, and the specific heat at constant pressure, and ϕ is the fraction of photon energy released as heat during deactivation.

Volume changes lead to the generation of sound waves that propagate in a medium to produce a pressure signal $p(t)$ at the surface of a pressure sensor. For different schemes of PA-conversion this signal may be directly calculated by using nonhomogeneous wave equation [2]. In the case with $i(t) = \delta(t)$ and $r(t) = \delta(t)$ (where $\delta(t)$ is the Dirac delta-function) the resulting acoustic signal represents the medium impulse response function $g(t)$ which describes the geometry of PA-experiment. In general, the acoustic signal $p(t)$ may be found as a convolution:

$$p(t) = \int_{-\infty}^{+\infty} g(t-\tau)\frac{\partial \nu(\tau)}{\partial \tau} FUN d\tau;$$

$$P(\omega) = G(\omega)V(\omega) \qquad (2)$$

where $G(\omega)$ is Fourier spectrum of $g(t)$ ($G(\omega)$ may be considered as a medium transfer function). Finally, the pressure is converted to an electric signal by a detection system, consisting usually of a pressure sensor and a high-impedance low-noise preamplifier. The impulse response of this detecting system $\gamma(t)$ should be convolved with the shape of the acoustic signal $p(t)$ to give an output voltage:

$$u(t) = \int_{-\infty}^{+\infty} \gamma(t-\tau)\, p(\tau) \mathrm{d}\tau;$$

$$U(\omega) = \Gamma(\omega) P(\omega) \qquad (3)$$

where $\Gamma(\omega)$ to the Fourier transform of $\gamma(t)$. Combination of expressions (1)–(3) gives a simple relationship between dynamics of deactivation and the output electric signal in the frequency domain:

$$U(\omega) = [\Gamma(\omega)G(\omega)I(\omega)]R(\omega)$$
$$= X(\omega)R(\omega) \qquad (4)$$

The function $X(\omega)$, incorporating the functions $\Gamma(\omega)$, $G(\omega)$, and $I(\omega)$, converts the relaxation spectrum to the spectrum of the output electric signal. This function describes all stages of PA-diagnostics and may be referred to as a 'photoacoustic filter'. Eq. (4) is the starting point of any time-resolved photoacoustic diagnostic problem. The inverse problem of PA-diagnostics may be now formulated as follows: to find relaxation spectrum $R(\omega)$ from experimentally detected spectrum of PA-signal $U(\omega)$, using a measured (or calculated) PA-filter $X(\omega)$. Expression (4) is typical of the general theory of linear systems [9]. Methods to solve the inverse problem expressed mathematically by convolution Eq. (4) will be discussed in detail in Section 4.

The proper choice of experimental set-up should ensure that the frequency pass-band of PA-filter $X(\omega)$ includes all frequency components of the relaxation spectrum $R(\omega)$. All elements of PA-diagnostics experimental scheme should be adjusted to this frequency band. It follows from (4) that one cannot benefit from a broad-band acoustic sensor while working with inadequate, slow impulse response configuration of PA-conversion and vice versa. The shape of the PA-filter $X(\omega)$ should be experimentally evaluated with a standard reference solution, but it is important to know how to estimate $X(\omega)$ theoretically for a proper choice of elements of the experimental set-up and for preliminary evaluation of possible results of relaxation dynamics restoration.

In this paper the case of PA-diagnostics of liquid samples with piezoelectric detection will be considered. The frequency band for such experiments may be roughly estimated by a low frequency limit of 50–200 kHz and a high frequency limit of 1–30 MHz. For more precise estimation one should calculate the functions $G(\omega)$ and $\Gamma(\omega)$. Appropriate expressions for these functions in several important cases are given below.

3. Evaluation of the PA-filter

3.1. Medium transfer functions

In PA-diagnostics two schemes of experimental set-up are generally used. One is intended for investigation of weakly absorbing liquids and implies cylinder-like configuration of the laser light absorption. The acoustic detector is located at a certain distance aside and its surface is oriented parallel to the laser beam axis [10]. This scheme will be referred further as 'cylindrical' (CL-scheme). In an-

other scheme the laser beam is directed normally onto a thin sample layer which is situated between a transparent window and a highly reflective mirror. The PA-signal is measured by a pressure sensor which is attached to the back side of a mirror [11]. For this scheme we shall use the term 'front face irradiation' (FFI-scheme), introduced in [11].

Cylindrical scheme

In weakly absorbing, transparent liquids the laser beam propagates in the sample medium without appreciable attenuation to form cylinder-like excitation region, which radiates cylindrical acoustic waves. In this case, as follows from calculations [12,13], the frequency dependence of $G(\omega)$ is given by:

$$G(\omega) = \rho_s \frac{\omega}{2} H_0^{(2)}\left(\frac{\omega}{c_s} r\right) D(\omega, a) \tag{5}$$

where r is the distance to the detector, ρ_s and c_s the density and the speed of sound in the sample, $H_0^{(2)}$ the Hankel function of the second kind, and $D(\omega,a)$ is the Hankel transform of cross-sectional distribution of the laser beam. For a Gaussian distribution (which corresponds to TEM_{00}-excitation mode), $D(\omega,a) = (a^2/2)\ \exp\{-(\omega a/2c_s)^2\}$, and for uniform beam $D(\omega,a) = a^2 J_1(\omega a/c_s)/(\omega a/c_s)$ (J_1 is the Bessel function).

For distances $r \gg a$, which are typical of PA-experiments, the frequency dependence of the function $G(\omega)$ is determined only by the beam radius a. The shape of $G(\omega)$ is shown in Fig. 1. Lower and upper frequency limits of the pass-band, defined approximately as points where $|G(\omega)| = 1/2$, are expressed through the characteristic frequency $\omega_0 = 2c_s/a$ as follows: $\omega_{c,\mathrm{low}} \simeq 0.1\,\omega_0$ and $\omega_{c,\mathrm{high}} \simeq 1.2\,\omega_0$ (for a Gaussian beam); $\omega_{c,\mathrm{low}} \simeq 0.15\omega_0$ and $\omega_{c,\mathrm{high}} \simeq 1.45\omega_0$ (for a uniform beam). For example, for radius $a = 1$ mm in aqueous solutions these frequencies for the Gaussian distribution are equal $\omega_{c,\mathrm{low}}/(2\pi) \simeq 48$ kHz and $\omega_{c,\mathrm{high}}/(2\pi) \simeq 573$ kHz. As follows from Fig. 1 uniform distribution gives broader transfer function for the same beam radius. However, this distribution is difficult to achieve experimentally, and existence of additional zero points makes the implementation of the restoration algorithm more complicated (see Section 4).

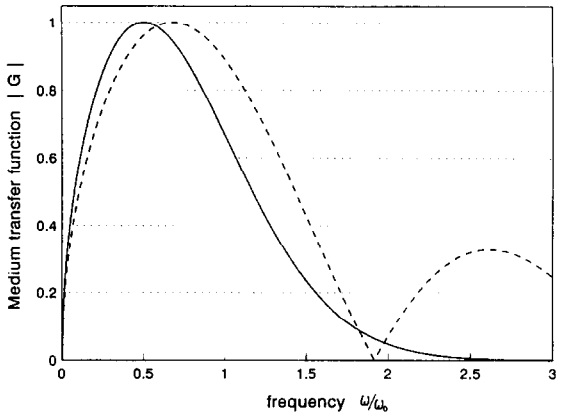

Fig. 1. Normalized medium transfer functions for CL-scheme of the PA- diagnostics in the case of the Gaussian cross-sectional distribution of laser intensity (solid line), and the uniform distribution (dotted line). Characteristic frequency $\omega_0 = (2c_s/a)$.

Front face irradiation scheme

Another scheme that may be used for PA-diagnostics of solutions with arbitrary light absorption utilizes a planar, layered configuration of excitation/detection. The laser beam is absorbed in the sample liquid layer which is confined between two other media. To avoid the problem of detector alignment the laser beam radius a in this configuration must be chosen large enough to meet the condition: $2c_s\theta z/a^2 \ll 1$, where θ is the laser pulse width, z is the distance from the sample surface to the detector. This ensures the planar geometry of excitation/detection scheme. Two limiting cases are of interest. First, when the light absorption coefficient of the sample μ is large enough, so that $\mu l \gg 1$, where l is the thickness of sample layer. In this case l can be chosen $c_s\theta \ll l$. Restricting observation by only directly transmitted pulse and neglecting multiple reflections on two interfaces, we can use the basic principles of calculations described in [14], and write out for $G(\omega)$:

$$G(\omega) = \rho_s \frac{i\omega}{(\mu^2 + k^2)} \frac{2}{1 + Z_b/Z_s} \times \left\{ \frac{i(Z_f/Z_s)\dfrac{\mu}{k} - 1}{1 + (Z_f/Z_s)} \exp^{-ikz} + \exp^{-\mu z} \right\} \tag{6}$$

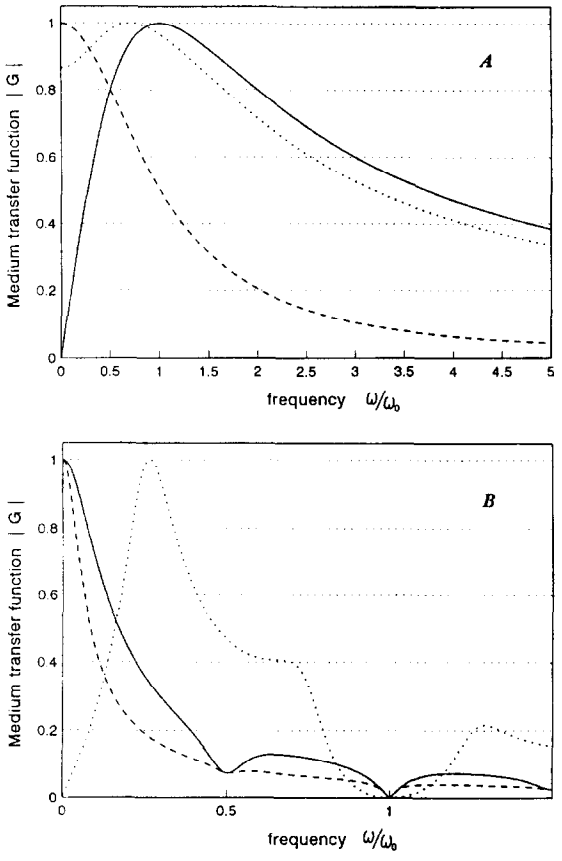

Fig. 2. Normalized medium transfer functions for FFI-scheme of the PA-diagnostics. (A) In the case $\mu l \gg 1$ (solid line: $Z_f/Z_s = 0$, dashed line: $Z_f/Z_s = 10$, dotted line: $Z_f/Z_s = 0.5$). Characteristic frequency $\omega_0 = \mu c_s$. (B) In the case $\mu l \ll 1$ (solid line: $Z_f = 13 \cdot 10^6$ kg/s/m^2 (quartz), $Z_b = 3.16 \cdot 10^6$ kg/s/m^2(lucite); dashed line: $Z_f = 13 \cdot 10^6$ kg/s/m^2, $Z_b = 8 \cdot 10^6$ kg/s/m^2; dotted line: $Z_f \approx 0$ (air), $Z_b = 3.16 \cdot 10^6$ kg/s/m^2). Sample medium was in all cases an aqueous solution. Characteristic frequency $\omega_0 = 2\pi(c_s/l)$.

where $Z_f = \rho_f c_f$, $Z_b = \rho_b c_b$, and $Z_s = \rho_s c_s$ are the acoustic impedances of the front, backing, and sample media, respectively; $k = \omega/c_s$ is the wave number of sound waves in the sample medium. The form of transfer function is quite different in two limiting cases of free ($Z_f/Z_s \to 0$) and constrained ($Z_f/Z_s \to \infty$) liquid surface (Fig. 2A). For this geometry of PA-conversion the function $G(\omega)$ is determined by the optical absorption coefficient. The correspondent characteristic frequency $\omega_0 = \mu c$. Cut-off frequencies for the case of a free surface are $\omega_{n,\mathrm{low}} = (2 - \sqrt{3})\omega_0$, $\omega_{n,\mathrm{high}} = (2 + \sqrt{3})\omega_0$. For a constrained surface boundary conditions: $\omega_{n,\mathrm{high}} = \omega_0$. For example, in an aqueous solution with $\mu = 100$ cm^{-1} one has $\omega_{n,\mathrm{low}}/(2\pi) = 640$ kHz, $\omega_{n,\mathrm{high}}/(2\pi) = 8.9$ MHz (for free boundary), and $\omega_{n,\mathrm{high}}/(2\pi) = 2.4$ MHz (for constrained boundary). It is worth noting that in the case of constrained (or finite impedance) boundary FFI-scheme provides a possibility to detect low frequency components down to $\omega \sim 0$. The presence of bottom medium for a limited observation time $t < l/c_s$ does not affect the PA-signal generation/detection.

In the other limiting case, the thickness of sample layer l is chosen to be small enough to obtain better time resolution [11]. For l in the range of tens of microns we can take $\mu l \ll 1$ even for an opaque sample; and consider that absorption along the z axis is uniform. This assumption is valid even for $\mu l \sim 1$ if bottom interface is totally light reflecting. Analytical expression for $G(\omega)$ may be written in the form [15]:

$$G(\omega) = \frac{\rho_s}{2} c_s^2 \frac{T_b}{i\omega} \left(\frac{1 - \frac{Z_s}{Z_f} T_f \exp^{-ikl} - R_f \exp^{-i2kl}}{1 - R_f R_b \exp^{-i2kl}} \right) \times \exp^{-i\omega(l/c_s - z/c_b)} \quad (7)$$

where transmission and reflection coefficients:

$$T_{f,b} = 2\frac{Z_{f,b}}{Z_{f,b} + Z_s}, \quad R_{f,b} = \frac{Z_{f,b} - Z_s}{Z_{f,b} + Z_s}$$

The transfer function $G(\omega)$ for some particular cases of different materials of front and backing layer are shown in Fig. 2B. The case when the front medium is absent is also presented for comparison. The upper frequency limit depends upon media impedances. For quartz front medium it is in the range $\omega_{n,\mathrm{high}} = (0.1\text{–}0.2)c_s/l$. For aqueous samples and thickness $l = 20$ μm it corresponds to the frequency range 7.5–15 MHz.

Estimations of limiting frequencies of the transfer function given in this section may be used for the proper choice of parameters of experimental set-up and evaluation of its working frequency band.

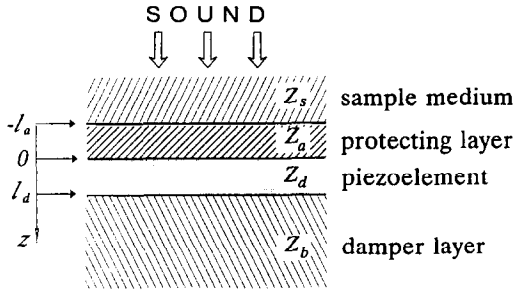

Fig. 3. Acoustic scheme of a thickness mode piezodetector according to the layered model.

3.2. Detection of the PA-signal

Detection of PA-signals induced in liquid samples by laser radiation is usually fulfilled by various type piezodetectors. Rigorous description of the acoustic pressure transformation to the electric signal depends on the configuration of detection scheme and the design of particular detector. A simple layered model for a thickness mode piezodetector gives adequate results in many practical situations [16,17]. In this model acoustic detector is considered as a layered structure in a direction of sound wave propagation (Fig. 3). This assumption is valid for pulsed measurements when the measured pressure pulse is short compared to the arrival time of reflections from the side walls of detector assembly. It is sufficient to take into consideration four media: front medium (liquid sample) with acoustic impedance Z_s; matching, protective layer (the impedance Z_a and the thickness l_a); piezoelement material (the impedance Z_d and the thickness l_d), and backing material or damper (impedance Z_b). Generalization of this model for a larger number of layers is also possible (for example, one can consider the impedance of the backing medium as an impedance of a layered structure).

Analytical expressions for the calculation of spectral sensitivity $|\Gamma(\omega)|$ of a thickness mode piezodetector are given in the Appendix. These expressions may be used to find the output voltage of the piezodetector in many experimental situations. For example in the case when the piezoelement is directly attached to the wall of the cell [18], the wall itself may be considered as a protective layer, and its thickness should be substituted for l_a in Eq. (A1) from Appendix. In Fig. 4A and Fig. 4B sensitivities of several variants of damped and resonant piezodetectors are displayed. Analysis of graphs in Fig. 4 shows that smooth spectral sensitivity may be obtained when impedances of the protective layer and backing medium are chosen as close as possible to that of the piezoelement. From this point of view a preferable choice is polyvinylidene fluoride (PVDF) sensors with an acoustically matched backing from Lucite or some plastic materials [16]. On the other hand, PVDF-sensors have comparatively low sensi-

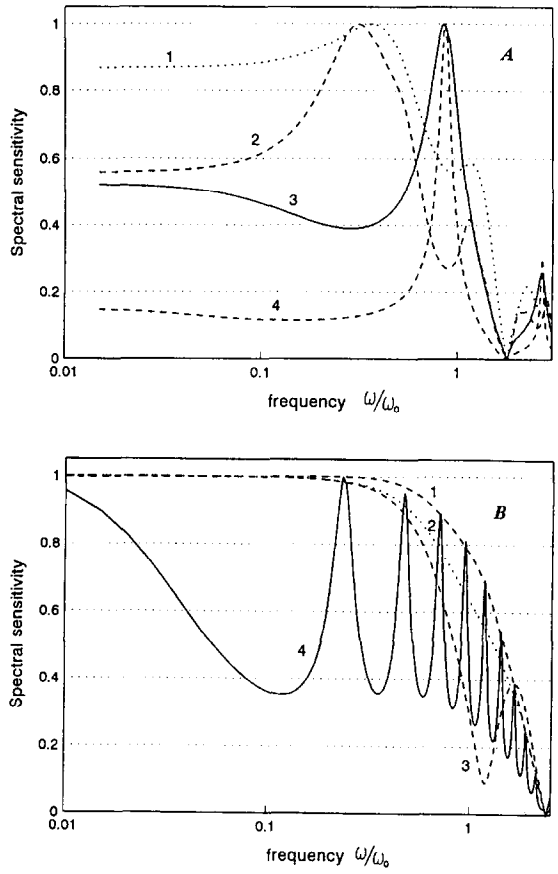

Fig. 4. Normalized spectral sensitivities of different piezodetectors. (A) PZT detectors with the structure: epoxy/PZT/lucite (curve 1), epoxy/PZT/brass (2), epoxy/PZT/Pyrex (3), Pyrex/PZT/brass (4). (B) PVDF-detectors with the structure: lucite/PVDF/lucite (1), lucite/PVDF/teflon (2), lucite/PVDF/brass (3), Pyrex/PVDF/lucite (4). Thickness of protective layer $l_a = 0.2$ mm for curves 1–3, and $l_a = 1.5$ mm for curve 4 on both graphs. Characteristic frequency $\omega_0 = 2\pi(c_s/2l_d)$.

tivity. For example, for typical case of a lead zirconate-titanate (PZT) ceramics detector with $l_d = 1$ mm and structure corresponding to curve 2 in Fig. 4A the sensitivity $|\Gamma|_{max} \simeq 65\mu V/Pa$, whereas for PVDF film of typical thickness 50 μm and the structure corresponding to curve 1 in Fig. 4B one has only $|\Gamma|_{max} \simeq 4\mu V/Pa$.

4. Restoration of relaxation kinetics

Theoretically, expression (4) provides an explicit method for calculating the spectrum $R(\omega)$ over the entire frequency range. In practice, the frequency range in which the spectrum $R(\omega)$ may be restored is limited by the presence of electric and acoustic noise in the detection system. In addition, for frequencies where $X(\omega) = 0$ no information about $R(\omega)$ can be restored. Even in the ideal case of noiseless detection the accuracy of calculation of $R(\omega)$ from (4) is limited by the precision of floating point operations in the computer program. The inverse problem of restoration of the relaxation kinetics, expressed mathematically by the convolution Eq. (4) belongs to the class of ill-posed problems [19–21]. The necessary condition of stability is not valid for this kind of problems: arbitrary small uncertainties in determination of spectrum $U(\omega)$ may lead to dramatic errors in restoration of the function $R(\omega)$. In addition, the solution of the problem is not unique [20].

There are several possible ways to solve the inverse problem. The choice of particular algorithm depends substantially on the information we have about the function to be restored. In the case when functional dependence of relaxation kinetics is known (for example, simple exponential decay), one can use iterative approximation procedures to find quantum yields and time constant in relaxation scheme [7]. In practice, however, the form of the PA-signal, especially for low-frequency, or resonant detection, does not provide explicit information about the underlying relaxation mechanism. In addition, in some complex situations the relaxation mechanisms are not yet understood, as in the case of PA-signal generation in water near 4°C [22,23], or in biological samples of bacterial reaction centers [5,8]. Thus, the PA-signal observed in water near 4°C was explained in Ref. [22] by the generation of sound by heated microparticles which are always present in a liquid, and in Ref. [23] by a structural relaxation of water clusters. In both cases the relaxation cannot be reduced to a simple exponential model and is governed by more complex equations. For these cases one should use a two-step approach to solve the inverse problem. In the first stage, explicit information about the relaxation kinetics $r(t)$ (or relaxation spectrum $R(\omega)$) should be extracted from the PA-signal profile. In the second stage, this information should be used to suggest a reasonable relaxation mechanism, and then parameters involved in theoretical scheme must be found by a nonlinear optimization algorithm.

An effective algorithm for solving this ill-posed problem is the regularization method, specially, Tikhonov's α-regularization [20,21]. This algorithm, which requires only continuity of the function $r(t)$, is designed to find some approximate solution which deviates minimally from the correct one (in the least square sense). The extent of inaccuracy will be determined by the noise figure of the detecting system. In a real experiment, instead of the expression (4), the measured output signal $\hat{u}(t)$ is related to the relaxation dynamics function $r(t)$ by the equation:

$$\hat{u}(t) = \int_{-\infty}^{\infty} x(t-\tau)\, r(\tau)\, d\tau + n(t)$$

where $n(t)$ is a function describing additive noise in the output of the detection system. For restoration of the relaxation function we have to use impulse response function $\hat{x}(t)$ that differs from real one $x(t)$ due to approximations used in its calculation or inaccuracy of its measurements. In general, given measured spectra $\hat{U}(\omega)$, $\hat{X}(\omega)$, the relaxation function $\hat{r}(t)$ may be found according to the formula:

$$\hat{r}(t) = \frac{1}{2\pi} \int_{-\infty}^{\infty} K(\omega) \frac{\hat{U}(\omega)}{\hat{X}(\omega)} \exp^{-i\omega t} d\omega$$

In this formula a special stabilizing factor $K(\omega)$ is included, which is different for different methods of restoration. It minimizes the root mean square deviation of the retrieved function from the real one. For the α-regularization procedure, the expression for $K(\omega)$ is given by [20]:

$$K(\omega) = \frac{|\hat{X}(\omega)|^2}{|\hat{X}(\omega)|^2 + \alpha Q(\omega)} \qquad (9)$$

where $Q(\omega)$ is a real non-negative even function of ω, and α is the parameter of regularization. The proper choice of $Q(\omega)$ and α ensures the stability of the restoration algorithm in the presence of noise and small deviations of restored functions $\hat{r}(t)$ and $\hat{R}(\omega)$ from the real ones [20].

The form of the function $Q(\omega)$ is determined by the features of the function $X(\omega)$, and should be examined separately in each particular case. Main consideration for the proper choice of $Q(\omega)$ is to ensure vanishing values of restoration filter $Y(\omega) = K(\omega)/X(\omega)$ for $X(\omega) \to 0$. After a choice of $Q(\omega)$, the regularization parameter α should be found in accordance with the uncertainty of the measured signal $\hat{u}(t)$. Let us designate the function $\hat{r}(t)$ restored with a particular value of α in (9) by $\hat{r}_\alpha(t)$ (correspondent spectrum $\hat{R}_\alpha(\omega)$). We can then introduce a measure for the deviation of the experimental signal $\hat{u}(t)$ from the signal that would correspond to the restored function:

$$\Phi(\alpha) = \int_{-\infty}^{\infty} |\hat{X}(\omega)\hat{R}_\alpha(\omega) - \hat{U}(\omega)|^2 \mathrm{d}\omega$$

If we know the standard deviation ξ of the PA-signal measurements:

$$\xi^2 = \int_{-\infty}^{\infty} |U(\omega) - \hat{U}(\omega)|^2 \mathrm{d}\omega$$

then, it may be shown that the optimal value of α is determined by equation:

$$\Phi(\alpha) = \xi^2 \qquad (10)$$

and that there exists a unique solution of this equation [20].

In general scheme of regularization there is one important particular case. Provided the power spectrum of uncorrelated frequency dependent additive noise $P_n(\omega)$ in the output is known exactly, it can be shown that the expression for the restoration filter is reduced to the formula for optimal Wiener filter [19,24]:

$$Y(\omega) = \frac{K(\omega)}{X(\omega)} = \frac{1}{X(\omega)} \frac{1}{1 + \dfrac{P_n(\omega)}{P_u(\omega)}}$$

where $P_u(\omega)$ is the power spectrum of noiseless PA-signal. In this case the procedure of restoration becomes optimal filtration.

As a result of the restoration procedure one obtains relaxation spectrum $\hat{R}(\omega)$ and correspondent function of the relaxation kinetics $\hat{r}(t)$. Regularization algorithm guarantees that both of these dependencies deviate from the real ones as little as possible for the given noise level. In fact, adequate restoration with the use of linear restoration algorithms is possible only in a limited frequency range where the function $X(\omega)$ is superior to noise. Information about spectral components of $R(\omega)$ that do not belong to this frequency range will be lost. Therefore, the broader the frequency band of the PA-filter $X(\omega)$, the more information about relaxation one can extract. Any additional information about the function to be restored (for example, positiveness of the solution) may be used to construct nonlinear algorithms with superresolving power. These algorithms enable to restore an information beyond the limits determined by signal-to-noise ratio (see [21,24] and references therein). Here we shall consider only more general linear methods.

In any case, part of the information about relaxation will be lost. Whether the measured signal is sufficient to determine well-defined values for the parameters which describe the process induced by the laser irradiation depends on both the quality of the data and the complexity of the model. For example, if the relaxation process is assumed to be described by a single exponential decay, characterized by an amplitude and relaxation time, these parameters can be restored even with a comparatively low-frequency experimental set-up [7]. For more complex cases of multiexponential decays or non-exponential relaxation it may turn out that restoration with two different set-ups will give quite different results and lead to irrelevant conclusions about the relaxation mechanisms. As an example the discussion about the nature of PA-signal in 4°C water may be referred [22].

5. Numerical modelling of restoration procedure

5.1. Principles of numerical simulation

The general procedure of numerical experiment simulating real process of relaxation dynamics

restoration was designed as follows (Fig. 5). The PA-filter $X(\omega)$ for two practical experimental set-ups were calculated (see next section for details). For the numerical modelling, the relaxation spectrum $R(\omega)$ was assumed to be described by a sum of exponentials. Functions $X(\omega)$ and $R(\omega)$ were then multiplied to give theoretical spectrum of the PA-signal $U(\omega)$. The PA-filter $X(\omega)$ and the spectrum $U(\omega)$ were inversely Fourier transformed (using FFT algorithm) to obtain theoretical impulse response function $x(t)$ and PA-signal $u(t)$. To simulate real experimental conditions normally distributed white noise with zero average $n(t)$ was added to both functions to give 'experimental' signals $\hat{x}(t)$ and $\hat{u}(t)$. The noise level was given by signal-to-noise ratio (S/N) determined by the expression:

$$S/N = \left\{ \frac{1}{T}\int_O^T u^2(t)\mathrm{d}t \Big/ \frac{1}{T}\int_O^T n^2(t)\mathrm{d}t \right\}^{\frac{1}{2}}$$

where $[0,T]$ is the time interval of the measurements.

We assume here, that spurious signals produced in the output of the detection system by electromagnetic pick-ups and laser light scattering can be measured and subtracted from the sample signal (see [11]). The presence of systematic errors in the experimental data makes a substantial problem for any restoration algorithm. This problem cannot be solved in the absence of information about the solution.

The block-diagram of numerical simulation in Fig. 5 depicts two approaches to the inverse problem solution. In the iterative approximation approach used in [7], experimentally detected function $\hat{x}(t)$ is directly convolved in the time domain with some model relaxation kinetics function $r_f(t)$ to get a fitted function $u_f(t)$ which should be compared with $\hat{u}(t)$. The implementation of the convolution in the time domain is forced by the usage of the resonant detector. In this case the time window of detection can cover only a part of the PA-signal. For accurate discretization of rapid relaxation functions, and experimental waveforms, comparatively fast sampling rate (10 ns) was needed [7]. For acoustically matched detectors described here, the sampling problem may be solved by implementation of the convolution in the frequency domain. In general, provided the measured signal $\hat{u}(t)$ has a non-zero value on the interval $[0,T_0]$, and its spectrum is band-limited, i.e. $\hat{U}(f) \simeq 0$ for all $|f| > f_{up}$ (this equality is approximate because finite function cannot have a strictly band-limited spectrum), the sampling theorem establishes the minimum number of points $N_{min} = 2f_{up}T_0$ which com-

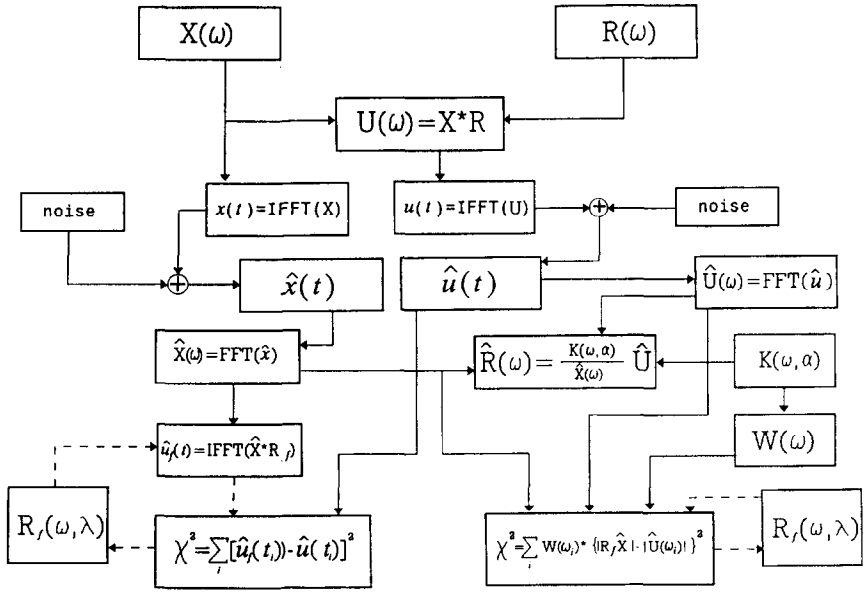

Fig. 5. Block diagram of the numeric modelling of the restoration procedure.

pletely determine the signal. In practice, one can take for nonlinear fitting an arbitrary number of point $N \geqslant N_{\min}$, as well as to calculate the spectrum at frequencies separated by an interval $\Delta f \leqslant 1/T_0$. This can be achieved by zero padding of the spectrum $\hat{U}(f)$ (for $f > f_{up}$), and the function $\hat{u}(t)$ (for $t > T_0$), respectively. The problem of the optimal choice of the number of points, and the sampling rate is discussed in the next section.

After some model of the relaxation kinetics is assumed, the final evaluation of parameters is made by one of the nonlinear optimization algorithms. In the case of iterative approximation one should minimize square of difference between PA-signal detected in the sample $\hat{u}(t)$ and the signal $\hat{u}_f(t)$ obtained by the convolution between model relaxation function $r_f(t)$ and impulse response of the system $\hat{x}(t)$ (Fig. 5). Calculation of χ^2 for estimation of goodness of the fit for iterative approximation is done according to:

$$\chi^2 = \sum_i \left[u_f(t_i) - \hat{u}(t_i) \right]^2 \qquad (11)$$

Summation in this expression is made over the points in the time interval of the measurements $[0,T]$ ($T \leqslant T_0$). The normalization on standard error for each digitization channel in (11) is omitted, because we use additive white noise with a fixed variance, and thereby deal with uniformly distributed errors.

Direct deconvolution by α-regularization algorithm implies calculation of stabilizer $K(\omega)$ in accordance with (9). For two practical experimental schemes of PA-diagnostics considered below appropriate calculations were made to establish the most suitable form of $Q(\omega)$ function. As reported in literature [24], in many cases it is enough to use polynomials in the form: $Q(\omega) = \Sigma\ c_i \omega^{2i}$ ($i = 1..M$). Function $Q(\omega)$ should ensure vanishing of the restoration filter $Y(\omega)$ for $\omega = 0$ and $\omega > \omega_{up}$ (above the upper frequency limit of the PA-filter $X(\omega)$). It was found that good results could be obtained with the function:

$$Q(\omega) = \left[\left(2.5 \frac{\omega}{\omega_{up}} \right)^2 - 1 \right]^{2n} \qquad (12)$$

for CL-scheme, and

$$Q(\omega) = \left[\frac{\omega}{\omega_{up}} \right]^{4n} \qquad (13)$$

for FFI-scheme. In these formulae $n = 1,2$. Value $n = 1$ gives smoother restored spectra while $n = 2$ leads to extension of the frequency band of restoration at the expense of increasing oscillations near the lower and upper frequency limits.

The optimal value of the regularization parameter α_{opt} was found as a solution of Eq. (10). Because $\Phi(\alpha)$ is a strictly monotonic function of α, it was sufficient to seek the optimal value α_{opt} by simple bisection algorithm [19]. Criterion to stop iterations was $[\Phi(\alpha)\text{-}\xi^2]/\xi^2 \leqslant 0.01\%$ (standard deviation ξ is equal in our case to the standard variation of random noise added to the signal). Optimal parameter α_{opt} along with the functions $Q(\omega)$ given by (12,13) were used to build stabilizer $K(\omega)$ according to expression (9).

The form of the stabilizer depends upon the noise level which thereby determines the possible frequency range of restoration. The frequency range may be derived from the shape of the stabilizing factor $K(\omega)$ which has sharp edges at frequencies f_l and f_h where the PA-signal becomes equal to noise. Therefore the limiting frequencies can be chosen as the points where relative declination of $K(\omega)$ dependence from the unity line is equal to a fixed tolerance, e.g. 1%. This is illustrated in Fig. 6, where upper frequencies f_h are marked by the arrows (for the calculation we used the PA-filters of two practical experimental set-ups described in detail in the next section). Theoretical analysis enables one also to implement precisely the procedure of optimal filtration. In Fig. 6 the stabilizing factors $K(\omega)$ for the restoration using the optimal filtration of the PA-signal for $S/N = 100$ are presented by dotted lines. As can be seen, the optimal filtration slightly extends the upper frequency of restoration at the expense of increasing oscillations of the solution near the limiting frequency so the actual upper limit will be practically the same as for α-regularization algorithm. Moreover, it should be stressed, that the optimal filtration is based on the information about the power spectrum of the noise and the noiseless PA-signal. This implies that the noise and the signal

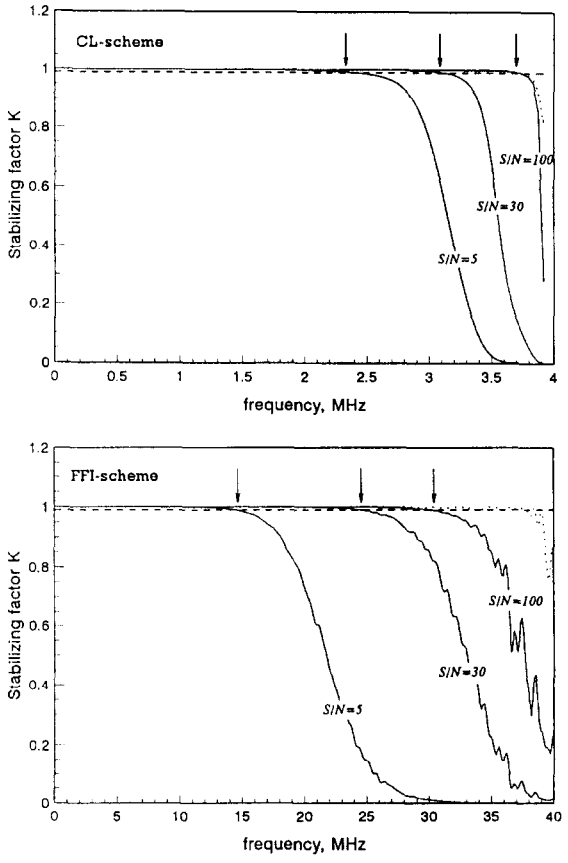

Fig. 6. Stabilizing factors in an α-regularization algorithm for the two schemes of the PA-diagnostics. Dashed lines show the tolerance 1% for determination of upper frequencies of restoration, marked by the arrows. Stabilizing factors for deconvolution by optimal filtration are shown by dotted lines.

can be separated (see the discussion in [19]) which is hardly the case in a real experiment.

The α-regularization algorithm uses the information about the noise to determine the frequency band of restoration. Therefore, in addition to the fitting of experimental waveforms in the time domain a possibility emerges to construct χ^2 in the frequency domain. The features of the stabilizing factor $K(\omega, \alpha)$ make it possible to form weighting function for the residuals: $W(f) = K(\omega, \alpha)$, $(f \in [f_l, f_h])$; $W(f) = 0$, $(f \notin [f_l, f_h])$. One can use this function to construct χ^2 in two ways: to fit the restored spectra $\hat{R}(\omega)$, or, alternatively, the experimental spectra $\hat{U}(\omega)$. Direct comparison of the results obtained by these two methods shows slightly better performance of the latter. Therefore, this method was chosen for numerical simulation and χ^2 was taken in the form:

$$\chi^2 = \sum_i W(\omega_i)\left(|\hat{U}(\omega_i)| - |\hat{R}(\omega_i)\,\hat{X}(\omega_i)|\right)^2 \quad (14)$$

where $\omega_i/(2\pi) \in [f_l, f_h]$.

5.2. Two practical schemes of the PA-experiment

To exemplify the general scheme of restoration we shall consider two different schemes of PA-detection for a typical set of experimental parameters.

The first, CL-scheme, implies cylindrical geometry of the PA-conversion. This scheme is widely used for PA-spectroscopy as well as for PA-diagnostics [5,10,18], and is suitable for diagnostics of weakly absorbing solutions. To obtain a better time resolution, one should focus the laser beam and attenuate laser energy to avoid nonlinear effects. This, in turn, leads to decreasing the S/N ratio. In practice, a reasonable upper frequency limit of the PA-signal detection may be estimated by value 1–3 MHz. The CL-scheme is rather simple in practical implementation, it is based on the usage of standard quartz spectroscopic cuvettes [5,7,18]. Parameters of the CL-scheme are mainly determined by the choice of the piezodetector. Of common use is the design described previously in [25], with a piezoelement being enclosed in stainless steel housing and loaded onto brass cylinder to provide acoustic matching. Such a detector is characterized by the upper frequency $f_{up} \approx c_d/2l_d$ (see Fig. 4A). Let us assume the frequency value $f_{up} = 2$ MHz (which may be approximately considered as an upper limit for piezodetectors of this type). Then, the thickness of piezoelement should be $l_d = c_d/(2f_{up})$ ($\simeq 1$ mm for PZT ceramics). As it follows from Figs. 1 and 4A in this case it is of no use to focus the laser beam below the radius $R = 2c_s/(2\pi f_{up})$ ($\simeq 0.25$ mm for aqueous solutions). Laser pulse profile for typically used Q-switched lasers may be taken as Gaussian with pulse width $\theta = 30$ ns. In general, the laser pulse duration always may be chosen short enough to be considered as a δ-pulse for PA-diagnostics experiments. For these parameters and appropriate electric loading of PZT-detector the resulting shape of PA-filter $X(\omega)$ is shown in the upper plot of Fig. 7.

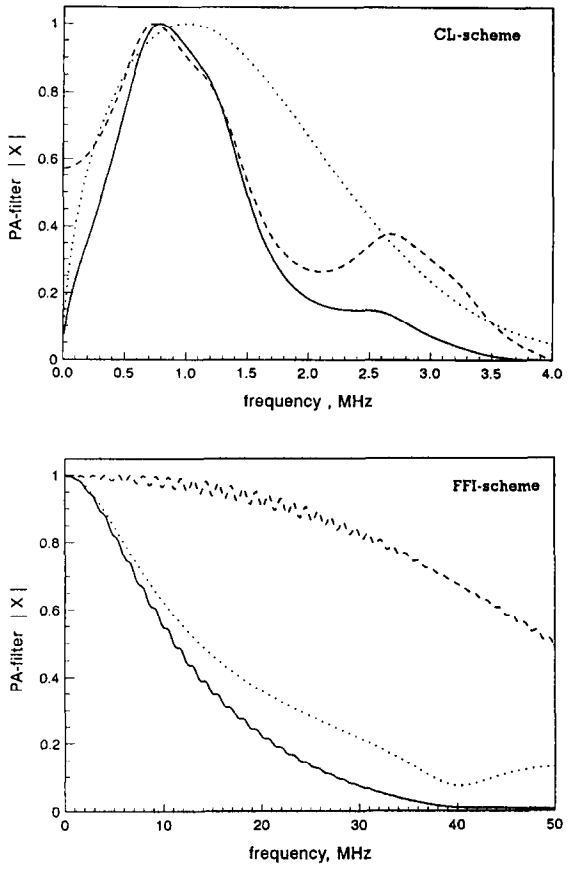

Fig. 7. Shape of the PA-filter X for the two schemes of the PA-diagnostics (solid lines). Corresponding medium transfer functions $|G|$ are shown by dotted lines, and spectral sensitivities of the detectors $|\Gamma|$ by dashed lines.

The second scheme represents experimental set-up for FFI-configuration. In this scheme the pressure sensor faces the laser beam and should be protected in some way. The FFI-scheme was theoretically considered in [26] and experimentally implemented in [11,27]. The advantage of this scheme is that one may probe solutions of arbitrary optical density. The time-resolution of this scheme is adjusted by the proper choice of the sample absorption or the thickness of the sample layer, as it was described in Section 3. As an example we shall consider a design similar to that used in [27]. Front medium on the scheme corresponds to a quartz window, backing medium is a totally reflecting mirror. The acoustic sensor is a broad frequency response PVDF-film sensor acoustically loaded onto a Lucite damper. Let us assume cut-off frequency of the sensor $f_{up} = 40$ MHz, that corresponds to the thickness of the film $l_d \approx 25$ μm. The best possible choice of material for the mirror (which constitutes protective layer for the piezodetector according to Fig. 3) is an acoustical equivalent to the damper material; i.e. Lucite. The thickness of this layer was chosen to be $l_a = 10$ mm for better separation of the main PA-signal from echo-signals. The sample layer thickness correspondent to the frequency band of the chosen PVDF-detector is calculated as $l_s \sim (c_s/c_d)l_d \approx 20$ μm. For this thickness, solutions with $\mu \leqslant 100\ \mathrm{cm}^{-1}$ may be considered as transparent, therefore expression (7) may be used to calculate PA-signal. The calculated shape of the PA-filter $X(\omega)$ for this case is shown in the lower plot of Fig. 7.

Characterization of complex photochemical and photobiological systems by the PA-technique starts with the acquisition of PA-waveforms. The shape of these waveforms depends upon the properties of the system under study, and the parameters of the experimental set-up. Any changes in the set-up will lead to some changes of the waveforms. Therefore, the PA-waveforms are not unique for a particular system, and cannot be directly compared, even if the same system was studied in two different labs by similar experimental set-ups. On the other hand, the restored relaxation spectra are specific to the particular system, and can be used for comparison of different systems (by analogy, for example, to acoustic attenuation spectra). An interpretation of these spectra is a separate task, which implies an accumulation of data under varying experimental conditions, and developing of a suitable theoretical model.

To illustrate this point, let us consider a complex multi-exponential decay in the form:

$$r(t) = \frac{A}{\tau_a}\exp\left(-\frac{1}{\tau_a}\right) + \frac{B}{\tau_b}\exp\left(-\frac{1}{\tau_b}\right) + C \quad (15)$$

where the parameters of relaxation kinetics: $A = 0.6$, $\tau_a = 1.5$ μs, $B = -0.4$, $\tau_b = 50$ ns, $C = 0.7$. The relaxation scheme in the form (15) is theoretically possible, for example, in photosynthetic samples, with negative amplitude B being correspondent to the photoinduced contraction [5,8] (it should be stressed, however, that there is no information about actual functional dependence of a structural relax-

ation in this case). The shapes of the PA-signals that would be detected in such a system by the two experimental set-ups considered above are presented in Figs. 8 and 9 (the shapes of corresponding impulse, responses are also shown for comparison by dashed lines). Without a-priori information about the decay one can hardly properly interpret the changes of the PA-waveforms. The results of the direct deconvolution of these waveforms in the two cases are shown in the lower plots of Figs. 8 and 9. Analysis of the relaxation spectrum restored by CL-scheme shows only the presence of all three decays, whereas broad-band reconstruction by the FFI-scheme enables to deduce the existence of unresolved fast relaxation (with $\tau_c < 5$ ns), and to estimate approximately the amplitudes and the relaxation times of two other decays.

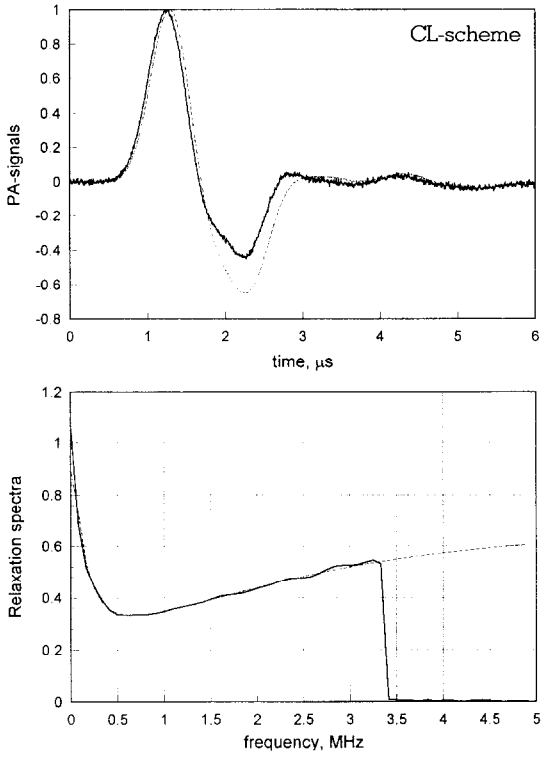

Fig. 8. Normalized PA-waveforms (a) and relaxation spectra restored from these waveforms by α-regularization algorithm (b) for the CL-scheme. Dashed line on the upper plot shows the impulse response function, on the lower plot the theoretical relaxation spectrum (the parameters of relaxation kinetics are listed in the text).

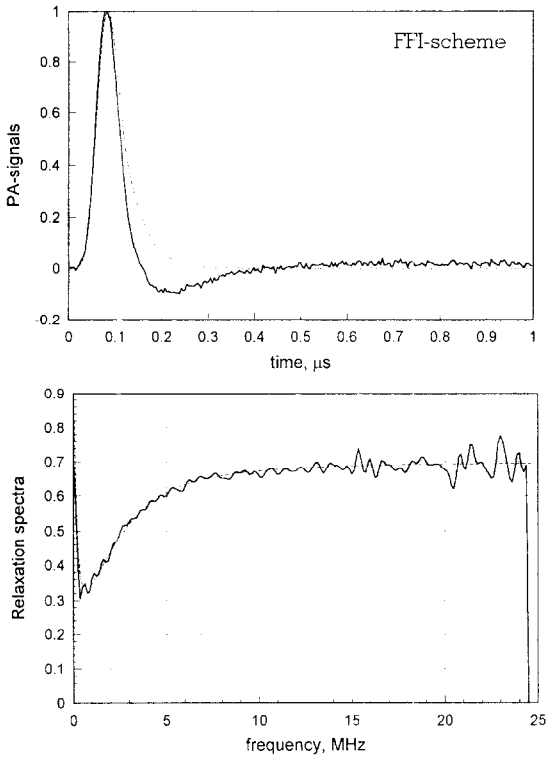

Fig. 9. Normalized PA-waveforms (a) and relaxation spectra restored from these waveforms by α-regularization algorithm (b) for the FFI-scheme. Dashed line on the upper plot shows the impulse response function, on the lower plot the theoretical relaxation spectrum (the parameters of relaxation kinetics are listed in the text).

The comparison of the PA-filter shapes for the two cases shows that the FFI-scheme of PA-diagnostics experiment potentially provides a much better frequency range of analysis, and a possibility to restore low-frequency components of the relaxation spectrum. This may be essential for adequate interpretation of restored data. On the other hand, the proper implementation of this scheme is a more difficult task. The gain in frequency range is reached in expense of the decrease in sensitivity, and thereby the S/N ratio. The two schemes were directly compared by numerical modelling described below.

5.3. *Time resolution of PA-diagnostics*

The question of the time resolution of PA-measurements is extremely important for the proper use

of the PA-technique. The time-resolution could be defined as an ability of the technique to discriminate between several relaxation processes, and to estimate corresponding time constants with an acceptable error. It is hard to formulate general quantitative criteria for the time resolution. General definition should take into account the features of relaxation kinetics, the parameters of experimental set-up, the quality of the measurements (S/N ratio), and the algorithm of the inverse problem solution. Here the possible influence of all these factors on the time resolution will be discussed.

As an example of the relaxation process let us consider two simultaneous exponential decays introduced by expression (15) (where $C = 0$). This case was extensively examined in PA-experiments [7,18,27,28]. Several definitions of the time resolution have been proposed. For cylindrical experimental set-up Braslavsky et al. [18,29] considered the time resolution to be equal to the transit time of the acoustic signal across the laser beam $2a/c_s$. Taking as an informative parameter the intensity of PA-signal, Terazima and Azumi [28] established the connection between this acoustic transit time and a range of relaxation times of slow decay that could be resolved from another fast decay. Barra et al. [30] proposed that good separation between fast and slow decays is possible when the lifetimes of the former have an upper limit of $\tau_D/5$ (τ_D is a time characterizing the impulse response of the detection system), whereas the energy-storage species should have a minimum lifetime of $5\tau_D$. Rudzki-Small et al. [7] reported that "two decay components may be adequately resolved, provided that the lifetimes are within the sensitivity range of the transducer and that the experimental noise level is sufficiently low". However, no quantitative criteria are presented. On the other hand, the authors consider their computer program to be able to analyze fast lifetimes of the order of the digitization channel width (till 10 ns).

As it can be seen, there is no acceptable general criterion for the time resolution even in the simplest case of bi-exponential decay. Therefore, it is relevant to study this case in more detail. Assume typical situation of one prompt heat release process, and another decay with finite time constant which should be resolved from the fast decay during PA-diagnostics. A set of parameters of the relaxation scheme were chosen to evaluate the performance of the two fitting algorithms and the two experimental set-ups. The block-diagram of numeric experiment is shown in Fig. 5. One relaxation process was taken as instantaneous ($\tau_a = 1$ ps). Three other parameters of the kinetic scheme (τ_b, A, B) were varied in broad range, and assumed to be free in the nonlinear least square fitting procedure. The experiment had to answer the question: what is the range of possible times τ_b, and the ratios of amplitudes B/A for which all three parameters could be restored with given confidence level for particular S/N ratio. The initial guess of parameters to be found is important for the success of any nonlinear fitting algorithm in the presence of noise, particularly when more than two parameters are fitted. Iterative approximation procedure, especially for low-frequency detection, should have considerable a-priori information about the system under investigation, and a close estimation of parameters to be found. As a rule, initial guess is based upon information obtained by other experimental techniques [3]. Direct deconvolution provides explicit information about relaxation and enables to evaluate relaxation parameters. Nevertheless, initial guess was chosen the same for both algorithms. Namely, five sets of the parameters A, B and τ_b were taken. Each set was formed by adding to the true value of the parameter random normally distributed numbers with variance which is equal to 50% of the parameter value. Then relative accuracy of restoration for each parameter was found, and an outcome of the experiment was evaluated by the lowest accuracy.

Numerical algorithms were implemented on MATLAB 4.2 software (Math Works, Inc.). The function LEASTSQ from MATLAB Optimization Toolbox v.1.0c was used for the nonlinear least square fitting (for details see [31]). As a rule, less than 100 iterations were necessary to find the solution.

To achieve better accuracy of restoration one should choose an optimal number of points for the fitting procedure, i.e. the time window of analysis and the sampling rate. The problem of the optimal choice has different percularities for the two experimental set-ups under consideration. In the case of CL-scheme the signals detected are finite in time for any time constant of the relaxation process (for

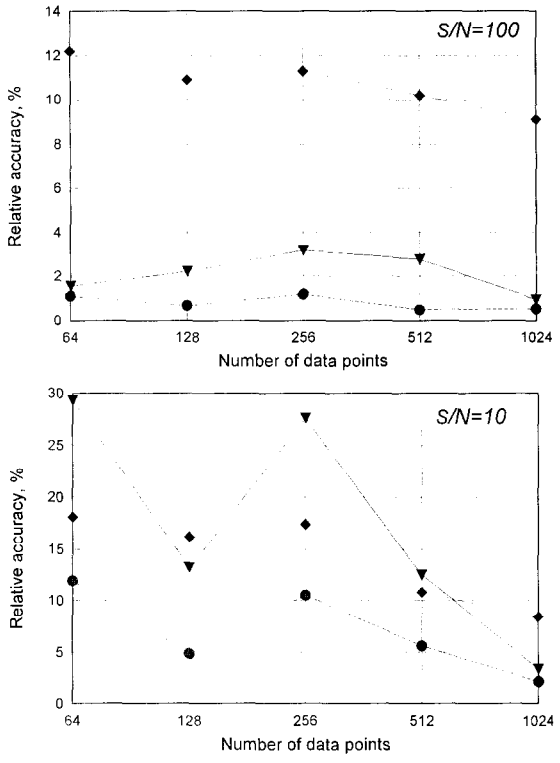

Fig. 10. Relative accuracy of the bi-exponential decay reconstruction by the CL-scheme for different numbers of sampling channels. The relaxation time constant τ_b: 50 ns (▼); 100 ns (●); 5 μs (◆). The amplitude ratio $B/A = 1.5$.

non-resonant detector the maximal duration of the signals is determined by the low-frequency limit of the PA-filter, and is equal in our case to $T \approx 11.5$ μs). Therefore, the problem is how many points on this interval one should take, with the minimum number being given by the sampling theorem ($N \approx 64$), and the maximum number by the number of digitization channels (we assume $N = 1024$). The dependencies of resulting accuracy of parameter retrieval are shown in Fig. 10 for two S/N ratios and different values of the relaxation time. These dependencies are not monotonic, there is a local minimum of the restoration error for $N = 128$. For large S/N ratios the accuracy of restoration is nearly the same for all sampling rates, whereas for poor S/N the increase of the number of points leads to the substantial improvement of the accuracy. In the case of FFI-scheme there is a possibility to detect very slow signals (the actual limit is imposed by the high-pass frequency of the electronics). Therefore, the question is how to choose the sampling rate for a given number of digitization channels $N = 1024$. For the fast sampling rates only a part of the signal is used for analysis, as it is shown in Fig. 11. The data in this plot were calculated under the assumption that the variance of the random noise is constant, and corresponds to the $S/N = 30$ and $S/N = 10$ respectively, for the time interval [0,300 ns]. Under these conditions the actual S/N ratio will drop when the sampling interval (and thereby the time window) is expanded. Therefore, the shape of the curves in Fig. 11 reflects a trade-off between the increasing part of the signal used for the fitting and the decreasing level of S/N.

As a result of optimization analysis for the iterative approximation algorithm, $N = 1024$ data points were chosen for the fitting. The time window of the PA-signal measurements was fixed for the CL-scheme ($T = 11.5$ μs), and properly adjusted for the

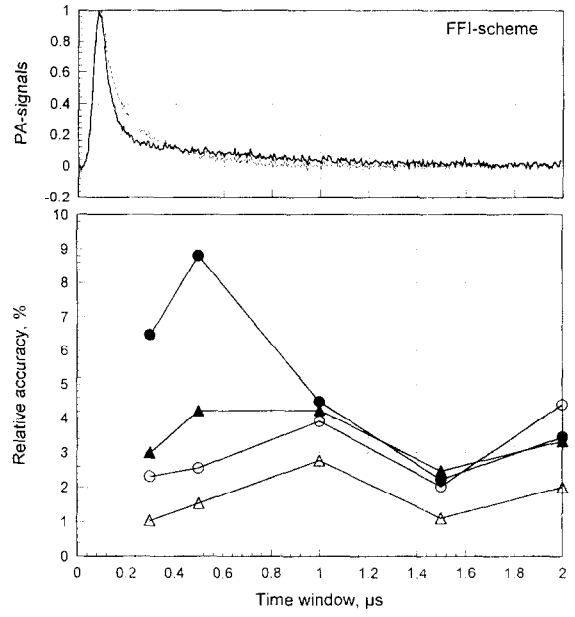

Fig. 11. Relative accuracy of the bi-exponential decay reconstruction by the FFI-scheme for different time-windows of the PA-signal detection. The relaxation time constants and S/N ratios: $\tau_b = 0.3$ μs, $S/N = 30$ (▲); $\tau_b = 0.3$ μs, $S/N = 10$ (●); $\tau_b = 0.1$ μs, $S/N = 30$ (△); $\tau_b = 0.1$ μs, $S/N = 10$ (○). The amplitude ratio $B/A = 1.5$. On the upper plot the PA-signal for $\tau_b = 0.1$ μs is shown by a solid line, and for $\tau_b = 0.3$ μs by a dashed line.

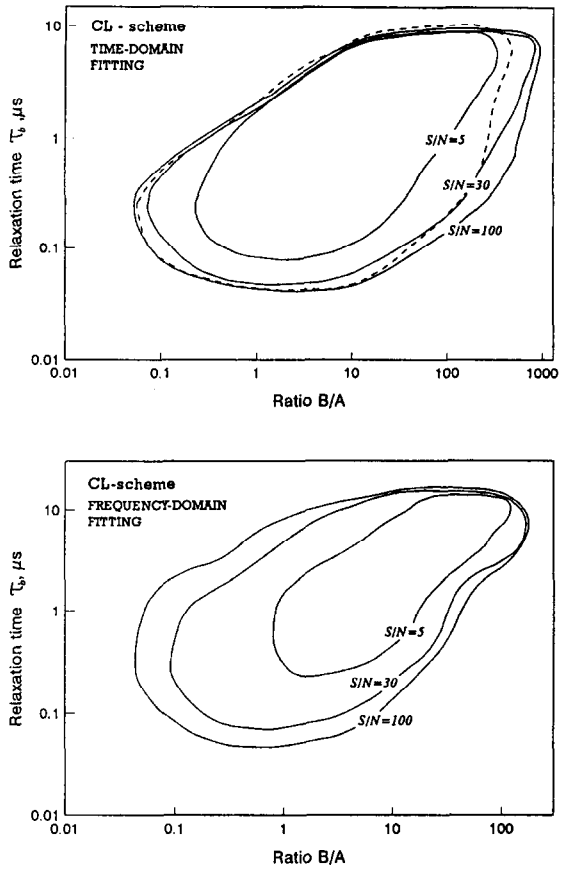

Fig. 12. The space of parameters of the bi-exponential decay that can be restored by the CL-scheme. Closed curves for various S/N correspond to the accuracy of reconstruction 10%, parameters inside the curves can be restored with better accuracy.

FFI-based scheme in the range $0.5 \leqslant T \leqslant 2$ μs to get the best accuracy. The value $T = 2$ μs was taken as a limit of distortion free observation time (this is a time window of the existing design of the FFI-cell described in [11]). In the case of direct deconvolution and subsequent fitting of the PA-spectrum, it was found that the best accuracy also corresponds to the maximum number of digitization points ($N = 1024$). Then the signal should be padded by trailing zeros till 8192 points for FFT spectrum calculation.

The results of numerical modeling for the two experimental set-ups and the two fitting algorithms are presented in area plots of Figs. 12 and 13. Closed curves on these plots comprise the area of τ_b and B/A values which can be restored for a given signal-to-noise ratio with the accuracy better than 10% (it was assumed that $B + A = 1$, so the ratio B/A gives a unique pair of B and A). Although the choice of quantitative criterion for a successful restoration is somewhat arbitrary, it was found that the positions of the curves in the area plots of Figs. 12 and 13 remain approximately the same for restoration errors in the range $5 < \epsilon < 20\%$. In other words, the accuracy of the restoration drops considerably even for a small declination of parameter values from those that determine the boundary of areas in the plots. Therefore, these plots give a good estimation of the parameters which could be restored in the case of bi-exponential decay.

Comparison of the area plots for different schemes and fitting algorithms shows some common features

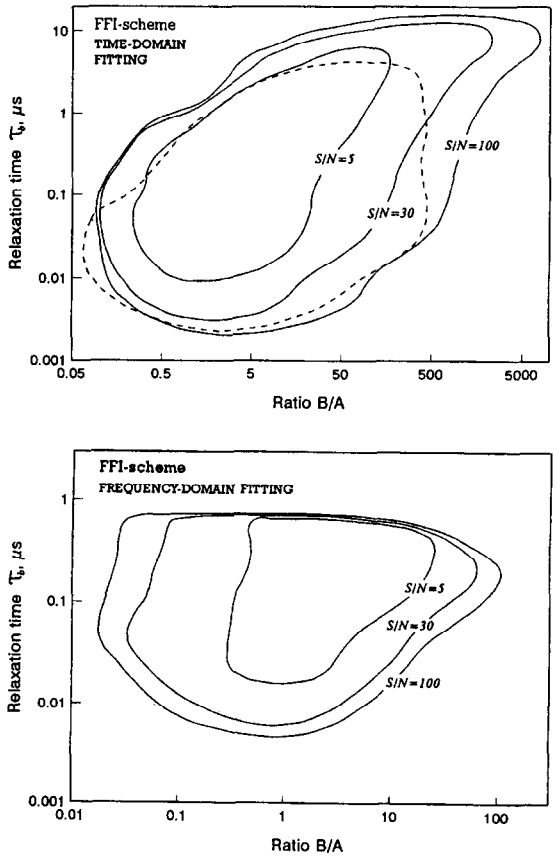

Fig. 13. The space of parameters of the bi-exponential decay that can be restored by the FFI-scheme. Closed curves for various S/N correspond to the accuracy of reconstruction 10%, parameters inside the curves can be restored with better accuracy.

of the reconstruction. For small relaxation time constant τ_b one can equally well resolve two components for both large and small B/A ratios (in the range 0.1–10), with the best resolution being correspondent to $B/A \sim 1$. In the case of CL-scheme, the increase of τ_b leads to the shift of the parameter values that could be resolved towards large B/A. Slow decays may be resolved only if their amplitudes B are 10–1000 times more than the amplitude of δ-functional decay. This effect can be explained by the fact that the efficiency of the sound generation for cylindrical configuration of PA-conversion is proportional to the time derivative of the heat release function. Therefore, the increase of τ_b and corresponding increase of B/A does not actually change the ratio of amplitudes of the PA-signals generated by the two components of the decay. The resolution of slow decays for both fitting algorithms is determined by the high-pass frequency limit of the PA-filter, and approximately equal to 11 μs. The resolution of the fast decays ($\tau_{b,\min} \sim 50$ ns for the time domain fitting, and $\tau_{b,\min} \sim 80$ ns for the frequency domain fitting) is much better than the limit imposed by the upper frequency of the PA-filter (~ 500 ns). It should be noticed also that there is no proportionality between the resolution and the sampling interval which equals 10 ns for all plots. Thus, for $S/N = 100$ the accuracy of reconstruction of the decay with $\tau_b = 50$ ns does not change substantially for the sampling rates from 10 ns till 160 ns (see Fig. 10).

The analysis of the area plots for the FFI-scheme shows that the resolution of the fast decay may be estimated $\tau_{b,\min} \sim 3$ ns for the time domain fitting and $\tau_{b,\min} \sim 5$ ns for the frequency domain fitting. The time constant corresponding to the upper frequency limit of the PA-filter in this case is equal to ~ 40 ns. Thus, in both experimental schemes, for large S/N there exists an approximate relationship between the minimal resolved time $\tau_{b,\min}$ and the upper frequency limit of the PA-filter f_{up}: $\tau_{b,\min} \sim 0.1/f_{up}$. As it was mentioned above, in FFI-scheme the maximal duration of the PA-signal detected by an ideally acoustically matched detector is theoretically limited only by high-pass frequency of electronics (i.e. preamplifier and amplifier). In practice, the time-window of the detection is determined by the time arrival of echo-signals reflected from unmatched interfaces inside the piezodetector housing. It is the time-window that determines the slow decay resolution for the time domain fitting: ~ 10–12 μs. By expanding the time-window, one can further improve the resolution. The limited time-window makes impossible to restore the slow decays (with $\tau_b > 0.8$ μs) by the frequency domain fitting, because of considerable distortions of the spectrum of the PA-signal.

One more consideration should be taken into account for the proper estimation of actual resolution of the slow decays. The area plots of Figs. 12 and 13 were calculated in the assumption that the energetic S/N ratio is constant in the whole range of relaxation parameters. In fact, for a practical purpose, it could be more convenient to consider the amplitude of the noise to be constant for particular experimental set-up. Then, for a slow decay and high B/A ratios where the efficiency of the sound generation drops substantially, the actual S/N will also decrease. Therefore, instead of the areas depicted in Figs. 12 and 13 by solid lines, one should use the areas plotted by dashed lines. These areas were calculated in the assumption that the level of the noise in the measurement of the impulse response was correspondent to the energetic $S/N = 100$, and then this level was assumed to be constant throughout the measurements. As it can be seen from Fig. 13, the noise level can practically limit the slow decay resolution of the FFI-scheme.

One of the possible experimental errors that could lower the accuracy of restoration is the time-shift of the reference point of the measurements. There are several possible reasons for that time-shift in real experiments. It is a small fluctuation of the time arrival of the triggering signal, the shift of the laser beam axis between experiments (in the case of CL-scheme). In addition, the variation of the sample temperature (this is necessary, for example, for the separation of different contributions to the PA-signal in the case of photosynthetic samples [5,8]), and its chemical composition also lead to the time-shift between the functions $\hat{x}(t)$ and $\hat{u}(t)$. For example, the change of water temperature on 1°C (around room temperature) leads to the variation of sound speed $\Delta c_s \simeq 3$ m/s [32], and, for an observation distance $r = 10$ mm (in the CL-scheme), to the corresponding time-shift ~ 13.6 ns. This shift is

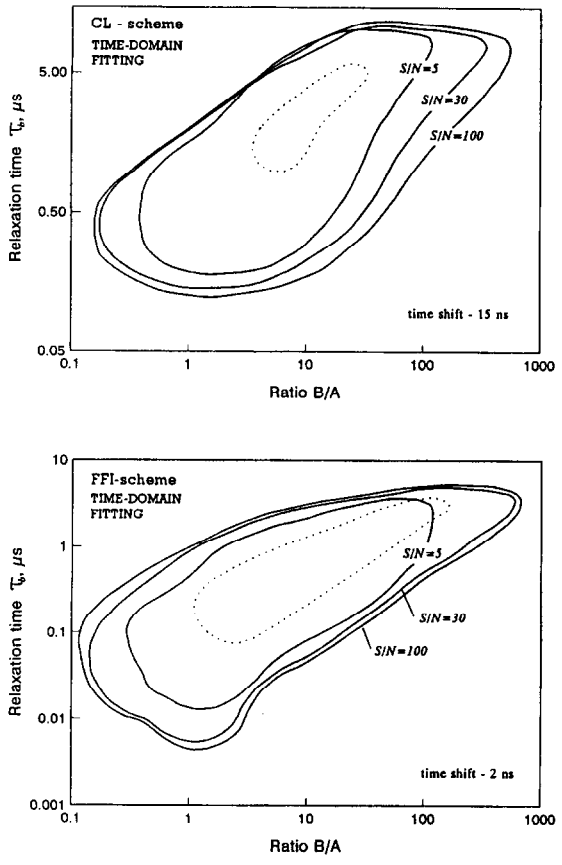

Fig. 14. The space of relaxation parameters that can be restored by the two schemes of PA-diagnostics when the reference and sample PA-signals are time-shifted.

quite small, and cannot be eliminated by the simple superposition of the PA-waveforms, because they are different for different relaxation times, and the starting point of the signal may be determined only approximately. The fitting in the frequency domain with χ^2 in the form (14) does not use phase information, and therefore, it is insensitive to the time-shift. The time domain fitting should take this shift into account, and incorporate in the fitting procedure one more parameter, namely, the time-shift between $\hat{x}(t)$ and $\hat{u}(t)$. In Fig. 14 the areas of parameters which can be found with 10% accuracy in the case of time-shifted signals are shown. The time-shift 2 ns was introduced for FFI-scheme and 15 ns (for the CL-scheme). These values are approximately equal to the sampling intervals in both cases. As it can be seen, the accuracy of restoration decreases appreciably, mainly because of the increasing number of parameters to be fitted, and corresponding complexity of χ^2 surface. If the correction for the time-shift is not made, the restoration could give completely wrong results (the areas of the relaxation parameters that still can be recovered are plotted in Fig. 14 by dotted lines for $S/N = 100$).

The results of numerical simulation lead one to infer that the preferable choice for the time-resolved PA-measurements would be the experimental set-up based on the FFI-scheme. For the comparable level of noise it gives much better resolution of fast decays than the CL-scheme, and also the larger dynamic range of the time constants that can be resolved. The main problem in practical implementation of this scheme is its low sensitivity. To achieve an acceptable S/N ratio one should consider the design with FET-probe preamplifier, which is built-in the detector housing in the vicinity of the PVDF-film [16]. A proper acoustic matching can improve the resolution of slow decays by the FFI-scheme, and extend the dynamic range of the time resolution till 10^4.

6. Conclusion

Analytical power of the PA-diagnostics is determined by its ability to cope with situations where minimal information about the genetics of the laser-induced relaxation processes is available. These situations are encountered in many complex photochemical and photobiological systems. Moreover, for the structural relaxation processes leading to the volume changes of non-thermal origin, the PA-diagnostics seems to be the only experimental technique available for analysis of the relaxation kinetics. This analysis should start with the direct deconvolution of the PA-waveforms, and obtaining of relaxation spectra. The spectra can be used for direct comparison of different samples and development of a suitable theoretical model of the relaxation. One of the linear algorithms of direct deconvolution, which has been considered here, is the Tikhonov's α-regularization algorithm that implies only continuity of the function to be restored. This algorithm gives explicitly the relaxation spectrum in the frequency band, where the PA-signal exceeds the noise; the frequency band

depends upon the parameters of experimental set-up, and the noise level. It has been shown, that the quality of the set-up may be described with the notion of the PA-filter, which transfers the relaxation spectrum to the spectrum of the output electric signal. Analytical expressions to calculate the PA-filter in various practical cases have been given. The direct deconvolution requires non-resonant detection of the PA-signal without any distortions. This, in turn, implies the usage of acoustically matched piezodetectors. The guidelines for the suitable design of PZT- and PVDF-detectors have been presented.

Once the relaxation spectra are interpreted, and some theoretical model of the relaxation is assumed, the parameters of the kinetics can be estimated by one of the nonlinear optimization algorithms. The fitting procedure can be implemented either in the time domain (iterative approximation), or in the frequency domain (after the direct deconvolution). To exemplify the general procedure of restoration, the relaxation kinetics in the form of bi-exponential decay has been assumed. This model turned out to be convenient for comparison of two widely used experimental schemes of the PA-diagnostics: cylindrical and front face irradiation scheme. The primary criterion chosen to estimate the performance of the particular PA-diagnostics scheme was the time resolution, which was considered here as an ability to resolve an arbitrary exponential decay from instantaneous δ-functional decay. Numerical modeling has shown, that for both experimental set-ups the time resolution of the fast decay for large S/N ratios is determined by the upper frequency limit of the PA-filter f_{up}. The minimal relaxation time that can be still resolved has been estimated as $\tau_{b,min} \sim 0.1/f_{up}$. The theoretical resolution of the slow decays depends upon the lower frequency limit of the PA-filter for the CL-scheme, and upon the time-window of the PA-signal detection for the FFI-scheme. In general, the FFI-scheme has evidently better time-resolution and the dynamic range of the relaxation times that could be restored. Despite low sensitivity, this scheme may be recommended for the time-resolved PA-diagnostics.

The choice of the fitting procedure (the time domain or frequency domain fitting) is mainly determined by the type of piezodetector. The advantage of the time domain fitting is the possibility to work with resonant PA-waveforms, and limited time-windows of the detection. However, it has been found that even small time-shift (in the order of the sampling interval) between the reference and the sample PA-signals can lower dramatically the accuracy of the reconstruction by this algorithm. Therefore, in practice the iterative approximation algorithm should explicitly incorporate this time-shift as a fitting parameter in the optimization procedure. The fitting of the amplitude PA-spectra is insensitive to the time-shift, but the frequency domain analysis requires the usage of acoustically matched detectors. Finally, the broad-band, distortion-free detection, which is essential for direct deconvolution, enables to combine the two fitting algorithms for reliable reconstruction of relaxation kinetics.

Acknowledgements

This work was made possible by post-doctoral fellowship of The Feinberg Graduate School, The Weizmann Institute of Science, and was supported in part by the Basic Research foundation of the Israel Academy of Sciences and Humanities and by the Willstatter center for photosynthesis. The author is grateful to Prof. Shmuel Malkin for constant support of this work and many valuable suggestions. Critical comments on the manuscript made by Dr. Vlad Brumfeld are also gratefully acknowledged.

Appendix A

We introduce here an expression for spectral sensitivity of a thickness mode piezodetector without derivation which is presented elsewhere [17]. Reflection and transmission coefficients on each interface shown in Fig. 3 are expressed through correspondent impedances as follows:

$$R_{a,b} = \frac{Z_d - Z_{a,b}}{Z_d + Z_{a,b}}; \quad R_s = \frac{Z_a - Z_s}{Z_a - Z_s}$$

$$T_{a,b} = \frac{2Z_d}{Z_d + Z_{a,b}}; \quad T_s = \frac{2Z_d}{Z_a + Z_s}$$

These coefficients will determine the propagation of

sound wave across the layered structure. Propagation factor describing transmission/reflection is given by:

$$K_{a,b} = \frac{\left(1 - \exp^{-i\omega\tau_d}\right)\left(1 - R_{a,b}\exp^{-i\omega\tau_d}\right)}{1 - R_a R_b \exp^{-i2\omega\tau_d}}$$

where $\tau_d = l_d/c_d$ is the propagation time of sound across piezoelement layer of thickness l_d and c_d the speed of sound in the piezoelement under the condition of zero electric induction $D = 0$.

To determine output voltage we should specify loading conditions. As a rule, high-impedance FET-probe preamplifiers are used for matching the piezoelement output and 50 Ohm standard cables. By designating input electric impedance of such a probe by Z_E, we may write for voltage transmission coefficient:

$$K_u = \frac{i\omega Z_E C}{1 + i\omega Z_E C}$$

where C is the capacitance of piezoelement. In the simple case of three media structure ($l_a = 0$) we have the following expression for the complex transfer function of the piezodetector:

$$\tilde{\Gamma}(Z_x) = -\frac{\dfrac{iK_xT_x}{\omega Z_d} h_{33} K_U}{1 + \dfrac{K_xT_x + K_bT_b}{2\omega^2 Z_E Z_d S} h_{33}^2 K_U}$$

where h_{33} is the piezomodulus $[N/C]$. In this formula index 'x' stands for designation of the medium directly adjacent to the piezoelement layer (it may be front medium or protective layer medium). In a general case of a finite thickness of the protective layer we have:

$$\Gamma(\omega) = \frac{\tilde{\Gamma}(Z_a)T_s \exp^{-i\omega\tau_a}}{1 + \left[\dfrac{\tilde{\Gamma}(Z_a)T_s}{\tilde{\Gamma}(Z_s)} - 1\right]\exp^{-i2\omega\tau_a}} \qquad \text{(A1)}$$

where $\tau_a = l_a/c_a$ is the sound propagation time for the protective layer (l_a is thickness, and c_a is the sound speed in the material of the layer). The absolute value $|\Gamma(\omega)|$ is referred as spectral sensitivity of the pressure detector.

It is worth to note that it is easy to take into account sound attenuation in the material of the layers and the piezoelement. One should substitute real values of wave numbers k_d, k_a by complex ones, with the imaginary part representing attenuation.

References

[1] S.E. Braslavsky and G.E. Heibel, Chem. Rev., 92 (1992) 1381.
[2] S.V. Egerev, L.M. Lyamshev and O.V. Puchenkov, Sov. Phys. Usp., 33 (1990) 739.
[3] K.S. Peters and G.J. Snyder, Science, 241 (1988) 1053.
[4] P.J. Shulenberg, M. Rohr, W. Gartner and S.E. Braslavsky, Biophys. J., 66 (1994) 838.
[5] S. Malkin, M.S. Churio, S. Shochat and S.E. Braslavsky, J. Photochem. Photobiol. B: Biol., 23 (1994) 79.
[6] J.A. Westrick, J.L. Goodman and K.S. Peters, Biochemistry, 26 (1987) 8313.
[7] J. Rudzki-Small, L.J. Libertiny and E.W. Small, Biophys. Chem., 42 (1992) 29.
[8] H. Arata and W.W. Parson, Biochem. Biophys Acta, 636 (1981) 70.
[9] S.L. Marple, Digital Spectral Analysis with Applications, Prentice-Hall, Englewood Cliffs, 1987.
[10] A.C. Tam, Rev. Mod. Phys., 58 (1986) 381.
[11] L.A. Melton, T. Ni and Q. Lu, Rev. Sci. Instrum., 60 (1989) 3217.
[12] H.G. Lai and K. Young, J. Acoust. Soc. Am., 72 (1982) 2000.
[13] J.-M. Heritier, Opt. Commun., 44 (1983) 267.
[14] V.E. Gusev and A.A. Karabutov, Laser Optoacoustics, Nauka, Moscow, 1991.
[15] M.I. Khan, T. Sun and G.J. Diebold, J. Acoust. Soc. Am., 93 (1993) 1417.
[16] O.B. Ovchinnikov, A.E. Pashin, O.V. Puchenkov and D.L. Rastorguev, Sov. Phys. Acoust., 33 (1987) 182.
[17] O.V. Puchenkov, PhD thesis, N.N.Andreev Acoustics Institute, 1990.
[18] S.E. Braslavsky and K. Heihoff, in J.C. Scaiano (Editor), Handbook of Organic Photochemistry, CRC Press, Boca Raton, vol. 1, 1989, p.327.
[19] W.H. Press, B.P. Flannery, S.A. Tenkovsky and W.T. Vetterling, Numerical Recipes: The Art of Scientific Computing, Cambridge Univ. Press, Cambridge, 1986.
[20] A.N. Tikhonov and V.Y. Arsenin, Methods of Ill-posed Problem Solution, Nauka, Moscow, 1979.
[21] G.Hammerlin and K.-H.Hoffmann, Improperly Posed Problems and their Numerical Treatment, Birkhouser Verlag, Basel, 1983.
[22] O.V. Puchenkov, J. Physique, IV-C7 (1994) 225.
[23] A.D. Pierce, J. Acoust. Soc. Am., Suppl. 1, 72 (1982) 513.
[24] G.I. Vasilenko and A.M. Taratorin, Image Restoration, Radio i Svyaz, Moscow, 1986.
[25] A.C. Tam and C.K.N. Patel, Rev. Mod. Phys., 53 (1981) 517.

[26] S.V. Egerev and O.V. Puchenkov, Sov. Phys. Acoust., 32 (1986) 30.
[27] L.G. Arnaut, R.A. Caldwell, J.E. Elbert and L.A. Melton, Rev. Sci. Instrum., 63 (1992) 5381.
[28] M. Terazima and T. Azumi, Bull. Chem. Soc. Jpn., 63 (1990) 741.
[29] K. Heihoff, S.E. Braslavsky and K. Scheffner, Biochemistry, 26 (1987) 1422.
[30] M. Barra, G.S. Calabrese, M.-T. Allen, R.W. Redmond, R. Sinta, A.A. Lamola, R.D. Small,Jr. and J.C. Scaiano, Chem. Mater., 3 (1991) 610.
[31] A. Grace, MATLAB Optimization Toolbox User's Guide, The Mathworks Inc., 1992.
[32] G.W.C. Kaye and T.H. Laby, Tables of Physical and Chemical Constants, Longman Group Ltd., 1973.